



AFRL-RZ-WP-TP-2012-0129

**TIME RESOLVED MAGNETO-OPTICAL IMAGING IN
HIGH FREQUENCY AC CURRENTS OF $\text{YBa}_2\text{Cu}_3\text{O}_{7-\delta}$ THIN
FILMS (POSTPRINT)**

Andrea Lucarelli, Alexander Frey, Ran Yang, and Gunter Luepke

The College of William and Mary

Timothy J. Haugan, George A. Levin, and Paul N. Barnes

Mechanical Energy Conversion Branch

Energy/Power/Thermal Division

FEBRUARY 2012

Approved for public release; distribution unlimited.

See additional restrictions described on inside pages

STINFO COPY

© 2006 Materials Research Society

**AIR FORCE RESEARCH LABORATORY
PROPULSION DIRECTORATE
WRIGHT-PATTERSON AIR FORCE BASE, OH 45433-7251
AIR FORCE MATERIEL COMMAND
UNITED STATES AIR FORCE**

REPORT DOCUMENTATION PAGE

Form Approved
OMB No. 0704-0188

The public reporting burden for this collection of information is estimated to average 1 hour per response, including the time for reviewing instructions, searching existing data sources, gathering and maintaining the data needed, and completing and reviewing the collection of information. Send comments regarding this burden estimate or any other aspect of this collection of information, including suggestions for reducing this burden, to Department of Defense, Washington Headquarters Services, Directorate for Information Operations and Reports (0704-0188), 1215 Jefferson Davis Highway, Suite 1204, Arlington, VA 22202-4302. Respondents should be aware that notwithstanding any other provision of law, no person shall be subject to any penalty for failing to comply with a collection of information if it does not display a currently valid OMB control number. **PLEASE DO NOT RETURN YOUR FORM TO THE ABOVE ADDRESS.**

1. REPORT DATE (DD-MM-YY) February 2012		2. REPORT TYPE Conference Paper Postprint		3. DATES COVERED (From - To) 01 January 2004 – 01 January 2006	
4. TITLE AND SUBTITLE TIME RESOLVED MAGNETO-OPTICAL IMAGING IN HIGH FREQUENCY AC CURRENTS OF YBa ₂ Cu ₃ O _{7-δ} THIN FILMS (POSTPRINT)				5a. CONTRACT NUMBER In-house	
				5b. GRANT NUMBER	
				5c. PROGRAM ELEMENT NUMBER 62203F	
6. AUTHOR(S) Andrea Lucarelli, Alexander Frey, Ran Yang, and Gunter Luepke (The College of William and Mary) Timothy J. Haugan, George A. Levin, and Paul N. Barnes (AFRL/RZPG)				5d. PROJECT NUMBER 3145	
				5e. TASK NUMBER 32	
				5f. WORK UNIT NUMBER 314532ZE	
7. PERFORMING ORGANIZATION NAME(S) AND ADDRESS(ES) The College of William and Mary Applied Science Williamsburg, VA 23187			8. PERFORMING ORGANIZATION REPORT NUMBER AFRL-RZ-WP-TP-2012-0129		
9. SPONSORING/MONITORING AGENCY NAME(S) AND ADDRESS(ES) Air Force Research Laboratory Propulsion Directorate Wright-Patterson Air Force Base, OH 45433-7251 Air Force Materiel Command United States Air Force			10. SPONSORING/MONITORING AGENCY ACRONYM(S) AFRL/RZPG		
			11. SPONSORING/MONITORING AGENCY REPORT NUMBER(S) AFRL-RZ-WP-TP-2012-0129		
12. DISTRIBUTION/AVAILABILITY STATEMENT Approved for public release; distribution unlimited.					
13. SUPPLEMENTARY NOTES Conference paper published in the proceedings of the <i>Materials Research Society Symposium</i> , Vol. 946, 2006. © 2006 Materials Research Society. The U.S. Government is joint author of the work and has the right to use, modify, reproduce, release, perform, display, or disclose the work. Work on this effort was completed in 2006. This paper contains color content. PA Case Number: AFRL/WSC 06-1085; Clearance Date: 06 Dec 2006.					
14. ABSTRACT We present a time-resolved magneto-optical (MO) imaging study of high-temperature superconductor (HTS) in high-frequency alternating current (AC) regime. The evolution of the magnetic flux density distribution in YBa ₂ Cu ₃ O _{7-δ} (YBCO) thin film samples is studied in small steps of the phase of the applied AC current. The flux distribution at 10 K exhibits instabilities including flux jumps and flux creep. A quantitative analysis of the data allows us to obtain the current density evolution. The current profile changes considerably with the phase differently from the prediction of the critical state model. These observations can be explained by the higher self-field at the sample edge and the effects of flux creep.					
15. SUBJECT TERMS time-resolved, magneto-optical, high-temperature superconductor, flux distribution, current density evolution, self-field					
16. SECURITY CLASSIFICATION OF:			17. LIMITATION OF ABSTRACT: SAR	18. NUMBER OF PAGES 12	19a. NAME OF RESPONSIBLE PERSON (Monitor) Timothy J. Haugan 19b. TELEPHONE NUMBER (Include Area Code) N/A
a. REPORT Unclassified	b. ABSTRACT Unclassified	c. THIS PAGE Unclassified			

Time Resolved Magneto-Optical Imaging in High Frequency AC Currents of $\text{YBa}_2\text{Cu}_3\text{O}_{7-\delta}$ Thin Films

Andrea Lucarelli¹, Alexander Frey¹, Ran Yang¹, Gunter Luepke¹, Timothy J. Haugan², George A. Levin², and Paul N. Barnes²

¹Applied Science, College of William and Mary, Williamsburg, VA, 23187

²Air Force Research Laboratory, Wright-Patterson, Ohio, 45433-7919

ABSTRACT

We present a time-resolved magneto-optical (MO) imaging study of high-temperature superconductor (HTS) in high-frequency alternating current (AC) regime. The evolution of the magnetic flux density distribution in $\text{YBa}_2\text{Cu}_3\text{O}_{7-\delta}$ (YBCO) thin film samples is studied in small steps of the phase of the applied AC current. The flux distribution at 10 K exhibits instabilities including flux jumps and flux creep. A quantitative analysis of the data allows us to obtain the current density evolution. The current profile changes considerably with the phase differently from the prediction of the critical state model. These observations can be explained by the higher self-field at the sample edge and the effects of flux creep.

INTRODUCTION

Currently, most estimates of the losses in superconductors rely on a nonlinear relationship between the current density and electric field $\vec{E} = \rho(|\vec{j}|)\vec{j}$ and assume that the temperature is fixed [1]. This implies that the induced electric field responsible for the losses changes on the same time scale as the applied magnetic field. However, recent investigations of the low-temperature superconductors reveal a much more intricate picture of flux penetration into a superconductor [2,3]. Flux jumps or thermomagnetic instabilities at low temperature in type-II superconductors are commonly observed which lead to dendritic avalanches developing over time scales much shorter than those determined by the ramping rate of the applied field [4-7]. The instability arises from the energy release due to the motion of magnetic flux that increases the local temperature thus decreases flux pinning and hence facilitates the further motion. The positive feedback can result in thermal runaways and global flux redistributions jeopardizing superconducting devices [8]. On longer times scales flux creep is also responsible for additional flux penetration [9]. As a result of highly nonequilibrium pattern of flux penetration the amount of losses in composite superconductors such as copper stabilized coated YBCO conductors may greatly exceed the traditional estimates.

In order to determine whether nonequilibrium pattern formation takes place in practical superconductors operating in the frequency regime of 10 - 10³ Hz it is necessary to use measurement techniques with inherent high time and spatial resolution capable of studying the dynamics of fluxons in a large area. A time-resolved magneto-optical (MO) imaging technique would be particularly effective due to the advantages of being both quantitative and fast. Here we report on time-resolved MO imaging measurements of YBCO thin films in the high-frequency AC current regime. Our results clearly show the presence of thermo-magnetic instabilities

leading to discrepancies in the magnetic profile and current evolution from the critical state model.

EXPERIMENTAL DETAILS

Our experimental setup, sketched in figure 1A, consists of a custom assembled Olympus polarizing microscope combined with a Janis ST-500 continuous-flow cryostat with an operating range of 3.5 to 325 K with a 50 mK stability. The cryostat has been specifically adapted to mount a permanent magnet or electromagnetic coil around a cold finger. A 0.4-mm thick sapphire window on top of the cryostat allows optical access to the sample. A 10x fluorite tension-free objective lens is used to minimize depolarization effects. A Glan-Thompson polarizer in combination with a linear polarizer provides an extinction ratio of approximately 10^{-5} . For time-resolved imaging, we use a Q-switched Nd:YLF diode-pumped solid-state laser which provides 100-nsec short pulses at 527-nm wavelength. The pulse repetition frequency (PRF) of the laser can be varied from single shot to 1200 Hz by an externally triggered Pockels Cell. We synchronize the laser PRF to the AC current frequency generated by a computer controlled power source in order to obtain time-resolved MO images of the current flow in the sample. We use a 6- μm thick epitaxial grown ferrite-garnet film (FGF) $(\text{Y,Bi,Pr,Lu})_{3.0}(\text{Fe,Ga})_{5.0}\text{O}_{12.0}$ with an in-plane magnetization as the MO indicator which is mounted on top of the HTS sample [10]. The iron garnet, depicted in the inset of Fig. 1, shows a pronounced Faraday rotation of about $1.08^\circ/\mu\text{m}$ for an external magnetic field of 750 Oe perpendicular to the film surface. Currently, the time resolution of our setup is determined by the jitter ($< 1 \mu\text{s}$) in the synchronization between the PRF and the AC current. Ultimately the time resolution achievable with this method will be limited to sub-nanoseconds by the magnetization switching time of the FGF as in ref. [11]. The power source provides up to 15 Amps of bipolar current in a customizable waveform at frequencies from 15 to 1200 Hz. Time-resolved images of the magnetic flux distribution in the superconducting sample are collected by a deep cooled charge-coupled device (CCD) camera.

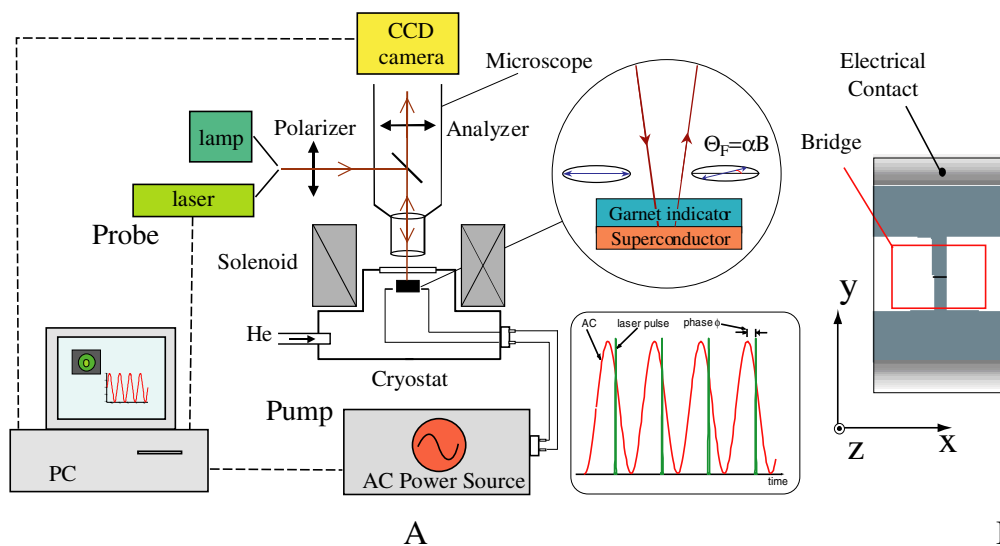


Figure 1. Schematic diagram of the time-resolved imaging setup (A) and the thin film sample (B).

The camera has a 12 bit dynamic range gray scale with excellent linearity and low dark current of 0.03 electron/pixel/sec. The effective area of the camera is 8.67 mm \times 6.60 mm consisting of 1344 \times 1024 square format pixels, 6.45 μ m in width. The camera which has a minimum exposure time of 10 μ s is interfaced to a PC which acquires the images at a maximum frame rate of 41 frames/sec.

The YBCO samples were grown by pulsed laser deposition on a LaAlO₃ or SrTiO₃ substrate with typical dimensions of 10 mm \times 5 mm [12]. The YBCO films are about 250-nm thick. The samples exhibit a critical transition temperature (T_c) of \sim 91 K, as determined by AC susceptibility measurements, and show a sharp transition within two degrees (at 2.2 Oe loss data). The samples are bridged (figure 1B) using a photolithographic technique with a length of 6 mm and a cross section $2w = 475 \mu$ m to reduce their critical current. Transport current measurements show a critical current density $J_c \sim 3 \text{ MA/cm}^2$ for the samples at 77 K. In the MO imaging experiments the YBCO sample is first cooled to the superconducting state down to 25 K in zero external field and then an external magnetic field of $B_a = 18 \text{ mT}$ is applied normal to the plane of the sample (z-direction). An AC current $I(t) = I_0 \sin(2\pi f t)$ is sent through the bridge of the sample (y-direction) and time-resolved MO images are taken at discrete values of the phase angle $\phi = 2\pi f t$. This is accomplished through an adjustable electronic time delay between the laser pulses and the applied AC current (inset of Fig. 1). An image with a good contrast requires an exposure time that covers two to ten laser pulses, depending on the intensity of the applied magnetic field. Thus the exposure time of the camera is adjusted according to the frequency of the AC current.

DISCUSSION

The top panel of figure 2 shows a sequence of images taken at $f = 1000 \text{ Hz}$ and $I_{peak} = 8.35 \text{ Amps}$ for different values of the phase. The white arrows in the images indicate the direction of the applied AC current. Small defects on the surface of the MO indicator are revealed in the images as dark spots. The images have been carefully calibrated to obtain a quantitative analysis of the measured intensities following the procedure described in [11]. The color scale on the right side of the top panel of figure 2 indicates the magnetic field intensity. Bright areas near the edges of the sample represent regions with high density of magnetic flux. The darkest part of the images are in the center of the bridge corresponding to a complete Meissner state. The magnetic flux tends to penetrate from the edge inside the sample as indicated in the images by the white region of maximum intensity that shifts from left to right as the phase changes from $\phi = -\pi/2$ to $\pi/2$. Moreover, there are three bright spots in the lower half of the right sample edge (marked a, b and c in Fig. 2). These magnetic flux lines do not move but change in density with the phase. They most likely result from flux jumps beyond the flux front. It has been shown recently that these instabilities occur when the background electric field E resulting from the Lorenz force exceeds a certain threshold E_c [8]. They develop in a nonuniform pattern if the background electric field E is high and the heat transfer coefficient to the substrate is small [8]. Furthermore, they can be driven by the ramping electric field due to the applied AC current. Local defects may also contribute to their occurrence.

In order to study the behavior of the magnetic flux as a function of the phase we consider the cross section profiles of the magnetic field intensities. The magnetic profiles shown in figure 2

(bottom) represent averages along the y-direction for the length of the image. For clarity, we plot magnetic profiles over half a period of the sinusoidal current with a phase increment of $\pi/6$. Due to symmetry, the images in the other half of the AC cycle nicely overlap with those shown in figure 2. The intensity and the position of both peaks of the flux profiles change considerably with the phase. At $\phi=0$ the magnetic profile due to the self-field of the superconductor should be symmetric. The observed subtle asymmetry most likely results from the small inhomogeneity of the applied field. At $\phi=-\pi/2$ the absolute maximum of the magnetic flux is near the left edge of the sample ($x/w \approx -1$). At the opposite edge, the magnetic flux forms a dip near $x/w \approx 1$ and the peak corresponding to the relative maximum is shifted further into the sample. The absolute maximum decreases while the relative maximum progressively increases as the phase changes from $\phi=-\pi/2$ to 0. This behavior is repeated on the opposite edge for $\phi=0$ to $+\pi/2$. The maxima move back and forth in the x-direction by about $70 \mu\text{m}$ during one cycle of the current which is due to the Lorentz force acting on the vortices. This corresponds to an average velocity of 0.14

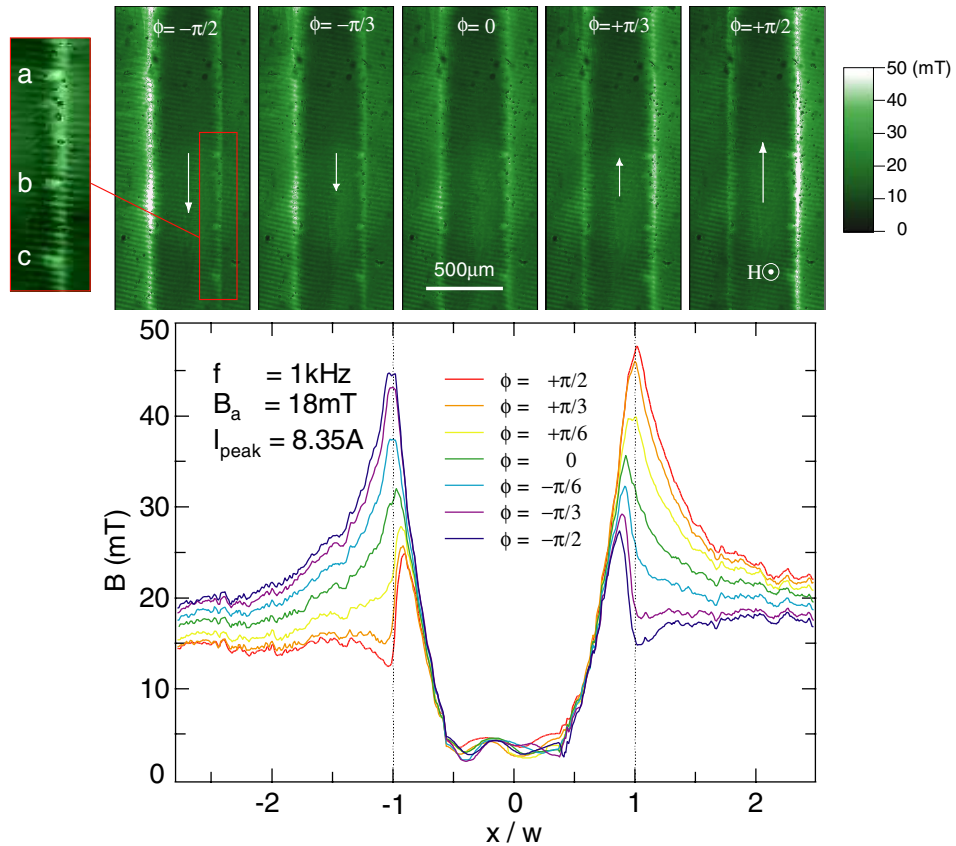


Figure 2. (Top panel). Time Resolved MO images for different values of the phase ϕ of the applied AC current. The white arrow in the images indicates the current flowing direction. The applied magnetic field is directed normal to the sample surface. The left inset shows an enlarged region of the right edge of the sample. (Bottom panel). Magnetic profiles for different values of the phase. The dashed lines indicate the sample edges.

m/s. This value is much smaller than the velocity associated with flux jumps but falls more into the range of flux creep velocity.

Despite the large changes of the magnetic flux profiles close to the edge of the sample the flux front penetration remains almost unchanged with the phase evolution differently from what the critical state model would predict [13]. This may be understood considering that the applied current is only $\sim 0.1 I_c$ and therefore its effect can be small compared to the screening current. On the other hand, magneto optical measurements with pulsed current [14] have shown also discrepancies from the critical state model which have been attributed to the presence of relaxation effects due to flux creep in the sample. Further modeling of the current evolution in the high-frequency AC regime is required to elucidate these effects.

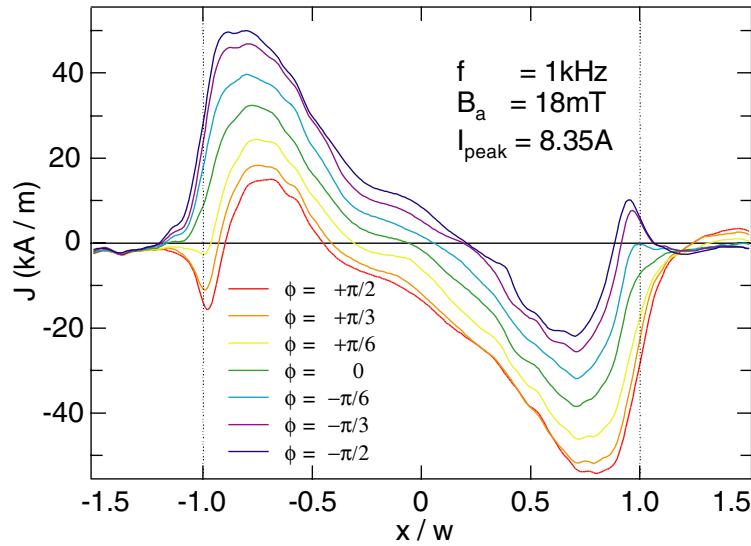


Figure 3. Current density profiles for different values of the phase. The inset shows the phase points chosen in the measurements.

Figure 3 presents the current-density distributions in the cross section of the bridge (x -direction) for different values of the phase ϕ . The curves are calculated from the measured flux-density distribution shown in figure 2 using a one-dimensional inversion scheme based on the Biot-Savart's law [11]. From this analysis we estimated an average distance $h = 6 \mu\text{m}$ between the indicator and the superconducting sample [11]. The accuracy of $J(x)$ near the sample edge is improved using the iteration procedure suggested in Ref. [14]. The final $J(x)$ presents a steeper drop at the edges and the component of the current density outside the sample is reduced to a negligible amount. Integration of the current density for $\phi = -\pi/2$ and $+\pi/2$ gives $I = 5.8$ Amps and 8.4 Amps, respectively, indicating reasonable agreement with the applied peak current of 8.35 Amps. The current density profiles change considerably with the phase. For example, when $\phi = 0$ there is no net current flowing through the sample and only the shielding superconducting current flows in a closed loop near the sample edges. The current profile at $\phi = 0$ is symmetric and the maxima correspond to J_c . At different values of the phase, a transport current flows through the sample in the positive or negative y direction (see top panel of figure 2) according to the polarity of the applied AC voltage. The transport current changes the overall current profile.

In a very simple picture we can consider the current densities shown in figure 3 as the sum of the screening current, due to the applied magnetic field, and the AC current. Then the current density at $\phi = 0$ represents the screening current and according to the critical state model its maximum value would be J_c . However, the maximum of the critical current changes with the phase differently from what the critical state model predicts [13]. Similar results have been obtained in MO imaging experiments with a pulsed current [14] and in simulations including flux creep [9]. Furthermore the maxima of the critical current are not at the sample edges as predicted by the critical state model. The critical current is reduced at the edges due to the higher self-induced magnetic field in that region as observed by recent experiment [15] and calculations [16,17]. In order to describe the observed discrepancies from the critical state model requires the inclusion of relaxation effects and thermo-magnetic instabilities.

CONCLUSIONS

In summary, we used a time-resolved MO imaging technique to study AC currents in HTS samples in the high-frequency regime. Time and spatially-resolved images of the magnetic flux profiles in a thin film YBCO sample are presented for different values of the phase. A quantitative analysis of the data allowed us to calculate the evolution of the current density with the phase angle. Our results reveal the presence of flux jumps and flux creep which can not be described by the critical state model.

ACKNOWLEDGMENTS

The work at CWM is supported in part by DOE grant DE-FG02-04ER46127.

REFERENCES

1. W.J. Carr, Jr, *AC Loss and Macroscopic Theory of Superconductors*, 2nd ed. (Taylor and Francis, London, 2001) and references therein.
2. I.S. Aranson *et al. Phys. Rev. Lett.* 94, 037002 (2005) and references therein.
3. I.A. Rudnev *et al. Appl. Phys. Lett.* 87, 042502 (2005) and references therein.
4. R.G. Mints and A.L. Rakhmanov, *Rev. Mod. Phys.* 53, 551 (1981).
5. A.V. Gurevich, R.G. Mints, and A.L. Rakhmanov, *The Physics of Composite Superconductors* (Begell House Inc., New York, 1997).
6. S.L. Wipf, *Cryogenics* 31, 936 (1991).
7. Martin N. Wilson, *Superconducting Magnets* (Clarendon Press, Oxford, 1983).
8. D.V. Denisev *et al. Phys. Rev. B* 73, 014512 (2006).
9. M.E. Gaeovski *et al. Phys. Rev. B.* 59, 9655 (1999) and references therein.
10. L.E. Helseth *et al. Phys. Rev B*, 64, 174406 (2001)
11. Ch. Jooss *et al. Rep. Prog. Phys.* 65, 651–788 (2002).
12. T. Haugan *et al J. Mat. Res.* 18(11), 2618 (2003).
13. E. Zeldov, J.R. Clem, M. McElfresh and M. Darwin *Phys. Rev B* 49, 9802 (1994).
14. A.V. Bobyl *et al Supercond. Sci. Technol.* 15, 82–89 (2002).
15. A. Lucarelli *et al. Supercond. Sci. Technol.* 19, 667–670 (2006).
16. S. Stavrev *et al. Supercond. Sci. Technol.* 18, 1300–12 (2005).
17. A. A. Babaei Brojny and J.R Clem, *Supercond. Sci. Technol.* 18, 888–95 (2005).